# Characterization of $NO_x$ Species Adsorbed on BaO: Experiment and Theory

**Peter Broqvist,* Henrik Grönbeck, and Erik Fridell**

*Department of Applied Physics and Competence Centre for Catalysis, Chalmers University of Technology, SE-41296 Göteborg, Sweden*

**Itai Panas**

*Department of Environmental Inorganic Chemistry, Chalmers University of Technology, SE-41296 Göteborg, Sweden*

*Received: August 27, 2003; In Final Form: January 15, 2004*

Charged $NO_x$ species ($x = 1,2,3$) formed upon adsorption of $NO_2$ on BaO are characterized by diffuse reflectance infrared Fourier transform (DRIFT) spectroscopy and theoretical vibrational analysis using the density functional theory (DFT). Experiments at 30 °C reveal nitrite formation. At $T > 250$ °C, shifts associated with formation of nitrates are observed, indicating an interconversion of oxygen atoms among adsorbates. The theoretical study includes single and pairwise $NO_2$ adsorption on $(BaO)_9$ clusters. As has been reported previously [Broqvist, P.; Panas, I.; Fridell, E.; Persson, H. *J. Phys. Chem. B* **2002**, *106*, 137], an additional energy gain is calculated for the second adsorbed $NO_2$. A vibrational analysis of the investigated adsorption configurations supports the interpretation of nitrite to nitrate interconversion on the BaO surface. Moreover, the calculations demonstrate the sensitivity in the $NO_2$ vibrational band splitting with respect to adsorption configuration.

## Introduction

Increasing emissions of green-house gases, mainly anthropogenic $CO_2$, have lead to the introduction of new strategies for the combustion of fossil fuels in transport applications. This will affect the choice of exhaust abatement system, since catalytic emission cleaning usually is performed after the combustion. Presently, the three-way catalyst (TWC) is employed for treating gasoline engine emissions. However, the TWC requires stoichiometric conditions to simultaneously catalyze oxidizing and reducing reactions, making it unsuitable in lean burn and diesel engine applications. Consequently, to increase the fuel economy while still preserving low emissions of locally harmful species (CO, HC, and $NO_x$), new catalytic strategies are needed. One such strategy is the so-called $NO_x$ storage and reduction (NSR) concept, introduced in the mid-1990s.[1,2]

The introduction of the NSR concept has increased the interest of alkaline earth metal compounds in the field of automobile exhaust after-treatment. For example, BaO is employed as a trapping agent for $NO_x$ emissions at lean combustion conditions. In an NSR catalyst, BaO, or more likely $BaCO_3$, and Pt are dispersed on a high surface $\gamma$-alumina support. The Pt/BaO/$Al_2O_3$ system has been investigated in several experimental studies, both under realistic conditions,[1−5] and with model catalysts using simplified gas compositions.[6−15] Important findings from these experiments are that NO is oxidized to $NO_2$ over Pt sites before the actual storage, and that the storage configuration is surface $Ba(NO_3)_2$.[8,10−12] These facts make it relevant to study $NO_2$ adsorption on BaO alone, thereby significantly reducing the complexity by removing the interaction between platinum and BaO.

In a previous study, we have performed density functional theory (DFT) calculations to explore possible mechanisms for the trapping of $NO_2$ on a BaO(100) surface.[16] In reference 16, a mechanism was proposed where $NO_2$ is initially adsorbed either on a surface oxygen or barium site, followed by the formation of surface nitrite−peroxo, nitrite−nitrate, and nitrate−nitrite pairs on the route toward the experimentally observed $Ba(NO_3)_2$ compound. The suggested storage mechanism is supported by kinetic modeling performed by Olsson et al.[8] and experimentally by Raman measurements of $NO_2$ storage on MgO-supported BaO performed by Hess and Lunsford.[13,14]

In reference 16, an enhanced stability was calculated for pairwise adsorption of $NO_2$ on the BaO(100) surface. The enhanced stability of pairwise adsorption was later shown to be valid on other alkaline earth oxides by studies of $NO_2$ adsorption on periodic MgO(100) slab models[17] and on $(MgO)_9$ and $(CaO)_9$ clusters.[18] In reference 18, a vibrational analysis was performed and characteristic vibrational properties of the adsorbed $NO_x$ species in different configurations were reported. However, because of the large differences in bond character and lattice parameters within the alkaline earth metal oxide series,[19] it is not clear whether results for $NO_x$ adsorption on MgO and CaO are directly relevant for BaO. This calls for a continuing theoretical study on the $NO_x$ interaction with BaO.

In the present work we study vibrational properties of $NO_x$ adsorbed on BaO by experiments and theory. The experimental approach includes diffuse reflectance FTIR (DRIFT) measurements of BaO and $BaCO_3$ powders exposed to $NO_2$. The theoretical study involves single and pairwise $NO_2$ adsorption on $(BaO)_9$ clusters. Experimentally, the degree of structural order in the storage material is unclear and the predicted difference in surface energy for the low index planes (100) and (110) of a BaO single crystal is small.[19] Consequently, large structural relaxation upon molecular adsorption is expected, which, for

* Corresponding author. E-mail: p.broqvist@fy.chalmers.se.

10.1021/jp036549c CCC: $27.50 
Published on Web 02/21/2004

example, has been demonstrated for Pt adsorption on BaO-(100).[20] Moreover, the structural properties of the adsorbate−MeO bond (Me being an alkali earth metal) has previously been found to be captured with a cluster description of the metal oxide.[21]

## Method

**A. Experimental Methods.** The DRIFT experiments were conducted using a BioRad FTS6000 FTIR spectrometer equipped with a continuous flow reaction chamber (Harrick Scientific Praying Mantis DRIFT optics and cell) and a mass spectrometer as described in ref 22. The experiments were performed with BaO and $BaCO_3$ powder samples.

The BaO powder (delivered from Strem Chem. Inc.) was as purchased 99.5% pure and the preparation of the reaction cell was conducted in a glovebox under a nitrogen atmosphere in order to avoid contamination by mainly $CO_2$ in the air. However, the background spectrum shows that the sample is to some degree contaminated by both hydroxy and carbonate species. Since only small contributions of hydroxyl are observed in the background spectrum, no preheating of the sample was conducted. This implies that initially, upon $NO_2$ adsorption, the disproportionation reaction $2OH^- + 3NO_2 \rightarrow 2NO_3^- + H_2O + NO$ probably will occur. This was observed during the measurements as weak negative bands in the spectra at the position of OH stretch modes. However, mass spectrometry did not show significant amounts of $H_2O$ or NO leaving the reaction cell upon the initial $NO_2$ adsorption sequence. The $BaCO_3$ sample (delivered from Aldrich) was as purchased 99.85% pure and prepared in air.

The experiments were performed by introducing 250 ppm $NO_2$ in Ar, with a total gas flow of 300 mL/min, over the powder sample. For BaO, two sets of experiments were done. The first set included 10 minutes of $NO_2$ exposure at 30 °C followed by a temperature ramp (∼5 °C/s) in Ar, with no $NO_2$ in the gas feed, to 500 °C with the background spectrum recorded at 30 °C. The second set was $NO_2$ storage at 250 °C with background spectra taken at this temperature. In case of $BaCO_3$, the measurements were performed by introducing $NO_2$ over the powder sample at 30 °C for 20 min. DRIFT measurements combined with mass spectrometric analysis where performed in situ. Due to the experimental conditions, only wavenumbers above 1000 $cm^{-1}$ were analyzed. Thus, we were not able to experimentally investigate the presence of surface peroxides, which are usually observed in the 900−800 $cm^{-1}$ range.[13]

**B. Theoretical Method.** The theoretical approach applied the DFT in the plane-wave and pseudo-potential (PW−PP) implementation.[23−26] The local exchange-correlation functional[27,28] was augmented with gradient corrections according to Perdew et al.[29] (GGA-PBE). Norm-conserving nonlocal pseudo-potentials[30,31] were employed together with a plane-wave basis set for the expansion of the valence electron wave functions up to a cutoff of 62 Ry. The calculations were performed in an embedding geometry consisting of a cubic cell (35 au) free from periodic boundary conditions.[32] Optimization of both electronic wave functions and atomic positions were performed via a direct inversion in iterative subspace (DIIS) method[33,34] and vibrational frequencies were calculated via numerical derivatives. The largest component of all gradients was converged below 0.02 eV/Å. The calculations of $NO_2$ adsorption on $(BaO)_9$ were performed spin restricted.

The theoretical approach was tested by calculations on bulk BaO and gas-phase $N_2$, NO, and $NO_2$.[35] In the tests, NO and $NO_2$ were calculated utilizing a spin polarized version of the density functional. The results are presented in Table 1. For the NO and $NO_2$ molecules, also a vibrational analysis was performed (cf. Table 2). The results are compared with experiments and all electron (AE) linear combination of atomic orbitals (LCAO) DFT calculations employing a double numerical basis set with polarization functions.[36,37] When comparing the PW−PP and the AE results, only minor differences are observed. Both techniques overestimate the experimentally observed binding energies and bond lengths for the molecules. For BaO in the bulk (only evaluated with PW−PP) the calculations underestimate the cohesive energy and overestimates the lattice parameter. This behavior is common for the GGA-PBE functional in comparison to experiments.[29] No clear trend can be found from the test on the vibrational properties upon comparison of the calculated wavenumbers using PW−PP or AE with experiments (cf. Table 2). For the NO molecule, the PW−PP calculations underestimate the experimental wavenumber by 2.0%, while the AE calculations overestimate it by 0.8%. For the $NO_2$ molecule, the symmetric stretch mode is underestimated using PW−PP (0.5%) and overestimated using AE (1.6%) while the bend mode is underestimated by ∼1.2% and the asymmetric stretch mode is overestimated by ∼2.5%, for both the PW−PP and AE results in comparison to experiments. From this analysis, the error in predicting experimental wavenumbers is in the range of ±3%, using the present computational techniques. Since we cannot predict the exact location of vibrational peaks, we instead focus on vibrational shifts and trends.

**TABLE 1: Results from Tests of the Computational Procedure[a]**

| | $E_{bond}$ [eV] | | | $d$ [Å] | | |
|---|---|---|---|---|---|---|
| | PW−PP | AE | exp.[39] | PW−PP | AE | exp.[38,39] |
| $N_2$ | 10.2 | 10.4 | 9.8 | 1.11 | 1.11 | 1.09 |
| NO | 7.1 | 7.3 | 6.5 | 1.17 | 1.16 | 1.15 |
| $NO_2$ | 4.1 | 4.2 | | 1.21 | 1.21 | 1.20 |

| | $E_{coh}$ [eV] | | a [Å] | |
|---|---|---|---|---|
| | PW−PP | exp.[40] | PW−PP | exp.[40] |
| BaO | 9.76 | 10.10 | 5.59 | 5.53 |

[a] The bond angles V(O−N−O) were calculated to be 134.2° and 133.4°, employing PW−PP and AE, respectively. The corresponding experimental bond angle for $NO_2$ is 134.3°.[38]

**TABLE 2: Wavenumbers for Calculated Vibrational Modes of Gas-Phase NO and $NO_2$**

| configuration | | $\omega_1$ sym [$cm^{-1}$] | $\omega_2$ bend [$cm^{-1}$] | $\omega_3$ asym [$cm^{-1}$] |
|---|---|---|---|---|
| NO | PW−PP | 1839 | | |
| | AE | 1891 | | |
| | exp[41] | 1876 | | |
| $NO_2$ | PW−PP | 1319 | 742 | 1648 |
| | AE | 1347 | 741 | 1652 |
| | exp[41] | 1325 | 750 | 1612 |

## Results and Discussion

This section starts with an analysis of spectra recorded during the DRIFT experiments followed by the computational results for $NO_2$ adsorption on $(BaO)_9$ cluster models. Thereafter, a discussion with interpretation of peaks observed in the DRIFT spectra based on the computational results and literature data will be given.

**A. Experimental Results.** *1. $NO_2$ on BaO.* Vibrational modes for BaO powder exposed to $NO_2$ were measured at 30 °C for 10 min. The recorded spectra are shown in the top panel of

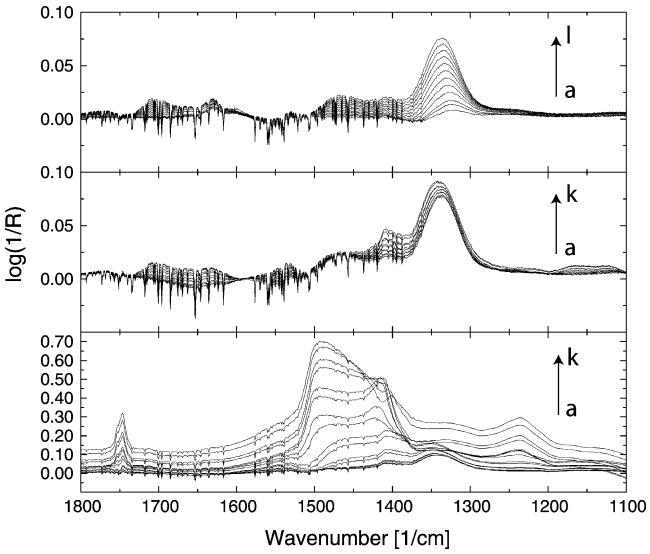


**Figure 1.** (Top panel) DRIFT spectra for 10 min of 250 ppm $NO_2$ exposure to BaO powder at 30 °C. The time interval is follows: a−c, 30 s; d−l, 60 s. Mid and bottom panels refer to the temperature ramp. (Mid panel) Temperature interval 30 °C to 150 °C where a−b are at 50 °C, c−d are at 70 °C, e−f are at 90 °C, g−h are at 110 °C, i−j are at 130 °C, and k is at 150 °C. (Bottom panel) Temperature interval 150 °C to 450 °C where a,b are at 200 °C, c,d are at 250 °C, e,f are at 300 °C, g,h are at 350 °C, i,j are at 400 °C, and k is at 450 °C. For the temperature ramp, spectra were taken every 60 s.

Figure 1. Initially, a major peak at 1319 $cm^{-1}$ and a broad peak centered around 1250 $cm^{-1}$ with low intensity are observed. The major peak shifts toward 1337 $cm^{-1}$ upon further $NO_2$ exposure. Broad peaks with low intensity are also observed in the ranges 1500−1400 $cm^{-1}$ and 1700−1600 $cm^{-1}$. The latter peaks could be assigned to physisorbed and gaseous $NO_2$ molecules, since these partly disappear when the $NO_2$ feed gas is turned off.

After 10 min of $NO_2$ exposure, the $NO_2$ gas is turned off and a temperature ramp in Ar is started. Spectra recorded during this ramp are given in the mid and bottom panels of Figure 1, where the mid panel refers to the temperature interval 30 °C to 150 °C and the bottom panel is the temperature interval between 150 °C and 450 °C. Initially, one observes a small shift of the major peak toward 1340 $cm^{-1}$ in conjunction with bands growing at ∼1410 $cm^{-1}$ (mid panel). These are increasing in intensity with higher temperature. A peak at 1750 $cm^{-1}$ emerges at a temperature of ∼250 °C (bottom panel). At this stage, the bands at ∼1410 $cm^{-1}$ are almost equal in intensity to that of 1340 $cm^{-1}$ and peaks are building up toward 1500 $cm^{-1}$ together with 1240 $cm^{-1}$. The changes in the vibrational spectra appear simultaneously with NO desorption detected by mass spectrometry. Upon further increase of the temperature (bottom panel) the spectra are dominated by a broad peak at 1500−1400 $cm^{-1}$.

The clear change in the character of the spectrum at ∼250 °C indicates the onset of surface reactions and triggered us to measure $NO_2$ storage at this temperature on a fresh BaO powder sample (cf. Figure 2). In this experiment, $NO_2$ was flowed continuously over the sample. The peaks at 1250, 1380, 1420, 1500, 1750, and 1780 $cm^{-1}$ are present from the start of the measurements. The peak at 1340 $cm^{-1}$, observed at lower temperatures (cf. upper panel in Figure 1) is not present, thus indicatative of temperature-mediated surface reactions of adsorbed $NO_2$. The peak structure is clearer than in Figure 1 since the number of surface species is larger and the background spectrum was measured at 250 °C (in Figure 1 the background spectrum was taken at 30 °C).

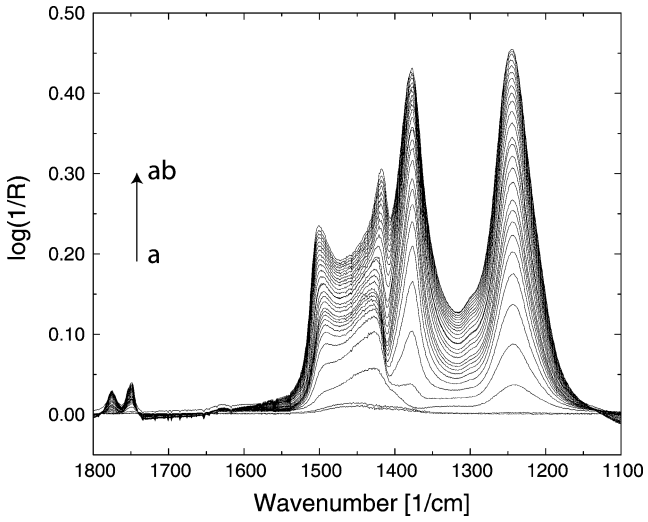


**Figure 2.** Spectra recorded for 30 min of $NO_2$ exposure to BaO at 250 °C. The time interval between each spectrum is: a−m, 30 s; m−q, 60 s; q-ab, 120 s.

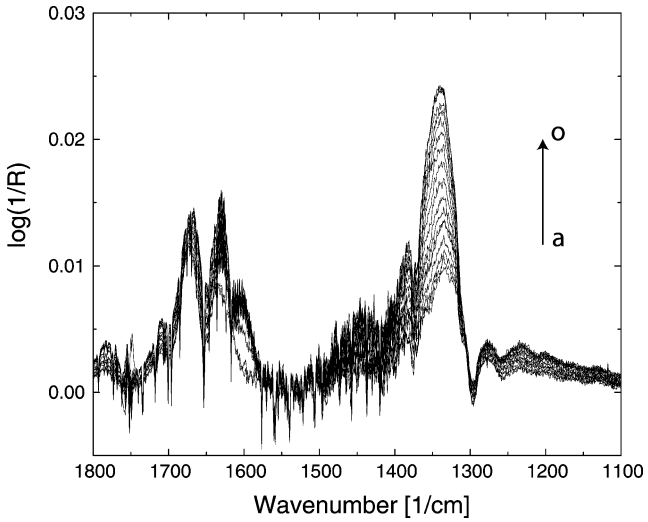


**Figure 3.** Spectra recorded for 20 min of $NO_2$ exposure to $BaCO_3$ powder at 30 °C. Time time interval between each spectrum is 30 s.

*2. $NO_2$ on $BaCO_3$.* As mentioned in the Introduction, BaO may not be present during $NO_x$ storage under real conditions, since BaO easily becomes carbonated, forming $BaCO_3$. Therefore, we conducted $NO_2$ storage experiments on a $BaCO_3$ powder sample in the same manner as described above. The spectra for $BaCO_3$ powder exposed to $NO_2$ at 30 °C are shown in Figure 3. The intensities are lower than for the BaO sample, which could be due to a lower accessible surface area, or, that a higher temperature is needed for decarbonation. However, just as for the low-temperature experiments on BaO, a major peak at 1340 $cm^{-1}$ is observed.

**B. Computational Results.** *1. Adsorption of One $NO_2$ Molecule.* Geometry optimizations were performed for two $(BaO)_9$ cluster configurations, one hexagonal (H) and one cluster cut from the solid NaCl structure (S). The two isomers have previously been found to represent relevant growth patterns for alkaline earth metal oxide clusters.[42] The two configurations are found to be nearly energetically degenerated, displaying an energy difference less than 0.01 eV, which is in agreement with previously reported data by Bawa and Panas using an LCAO DFT technique employing Gaussian basis functions.[42]

In our previous calculations,[16] $NO_2$ was found to adsorb with highest adsorption energy over surface oxygen ions. On the

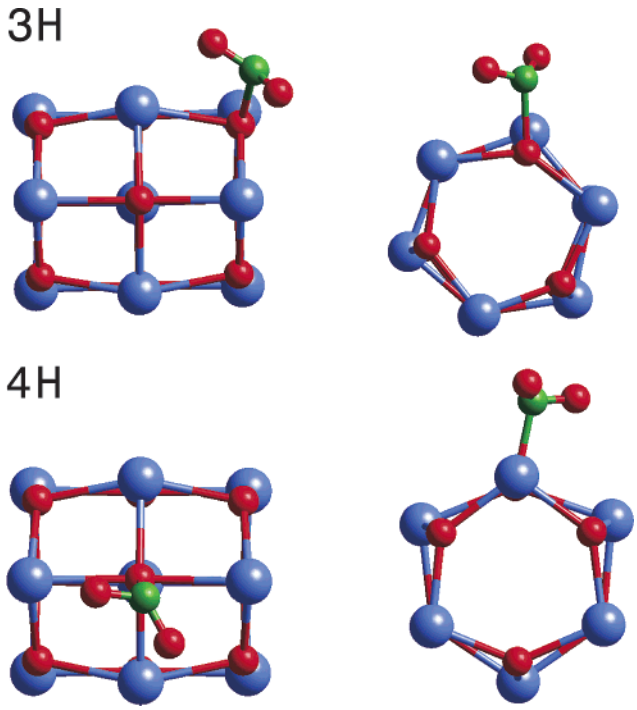


**Figure 4.** $NO_2$ adsorption on $(BaO)_9$ in the hexagonal configuration, top and side views. Blue is Ba, red is O, and small green is N.

**TABLE 3: Results from Geometry Optimization Calculations of Single $NO_2$ Adsorption on $(BaO)_9$ Cluster Models. (The different geometrical configurations are illustrated in Figures 4 and 5.)**

| | 3H | 4H | 3S | 4S | 5S |
|---|---|---|---|---|---|
| $E_{ads}$[eV] | −0.93 | −0.99 | −0.94 | −1.34 | −1.35 |
| R(N−O) [Å] | 1.25 | 1.26 | 1.25 | 1.27 | 1.27 |
| R(N−$O_{surf}$) [Å] | 2.06 | 2.24 | 2.07 | 2.83 | 2.75 |
| V(O−N−O) | 123° | 122° | 122° | 118° | 117° |

studied clusters, three different oxygen sites exist; 3-, 4-, and 5- coordinated. $NO_2$ adsorption was investigated over all these sites. The different geometrical configurations are shown in Figures 4 and 5, and the corresponding adsorption energies and structural data are reported in Table 3. The two three-coordinated sites, 3H and 3S, were found to have similar adsorption energies for $NO_2$.

The 4S and 5S configurations are found to be significantly more stable than the 4H configuration. This is most likely owing to both steric and charge donation effects. In the 4S and 5S configurations, the $NO_2$ molecule is adsorbed with the nitrogen over the oxygen site, allowing the two $NO_2$ oxygens to create bonds to two barium cations. In the 4H configuration, the $NO_2$ oxygen is only capable of efficient binding to one barium site (compare Figures 4 and 5). Moreover, by comparing the O−N−O bond angle for the adsorbed $NO_2$ molecules among these configurations, we conclude that the more nitrite-like (angle close to 117°) the adsorbed species become, the higher is the adsorption energy. We also investigated the adsorption of $NO_2$ over a cation pair site (no $O_{clus}$−N bond) reported to be the most stable configuration for $NO_2$ on MgO(100) slabs,[17] $(CaO)_9$ clusters,[18] and on BaO(100) modeled by an embedded cluster technique.[43] Our calculations indicate that this geometry is meta-stable, being ∼0.15 eV less stable than the 5S configuration.

Two of the studied adsorption configurations were chosen for vibrational analysis, namely the 3S and 5S clusters (cf. Figure 5). In the 5S cluster the $NO_2$ is adsorbed as a nitrite, whereas in the 3S cluster the $NO_2$ molecule is adsorbed in a

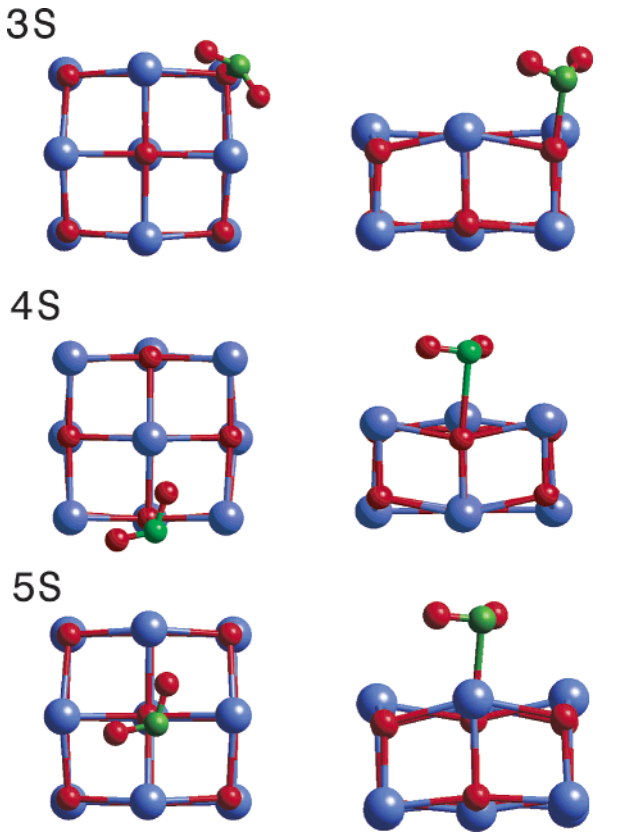


**Figure 5.** $NO_2$ adsorption on $(BaO)_9$ in the slab configuration, top and side views. Same color code as in Figure 4.

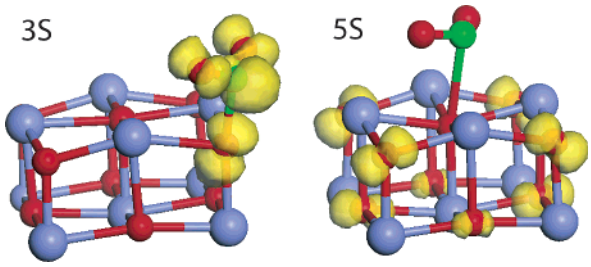


**Figure 6.** HOMO density for the 3S and the 5S configurations. The isosurface is at ±0.04 eV/Å. Same color code as in Figure 4.

**TABLE 4: Wavenumbers for the Calculated Vibrational Modes for an Adsorbed $NO_2$ Molecule in the 3S and 5S Configurations**

| configuration | $\omega_1$ sym [$cm^{-1}$] | $\omega_2$ bend [$cm^{-1}$] | $\omega_3$ asym [$cm^{-1}$] |
|---|---|---|---|
| 3S | 1210 | 729 | 1384 |
| 5S | 1304 | 770 | 1299 |

strained $NO_3^{2-}$ configuration. The assignments of the nitrite and the $NO_3^{2-}$ species are done on the basis of the bond angle (V(ONO)) and the character of the highest occupied molecular orbital (HOMO) density, cf. Figure 6. $NO_2$ has an unpaired electron, and upon formation of a nitrite, an electron must be transferred from the surface to the $NO_2$. This is the case for the 5S configuration, where the HOMO density is delocalized over the cluster oxygen ions, indicating nitrite formation. The 3S HOMO density, localized over the oxygen adsorption site and the adsorbed $NO_2$ molecule, signals a $NO_3^{2-}$ species.

The vibrational wavenumbers associated with $NO_2$ in the 3S and 5S configurations are reported in Table 4. As expected (on the basis of the HOMO density plots), a large difference is observed between these two configurations. The wavenumber difference in the 3S configuration, i.e., the difference between

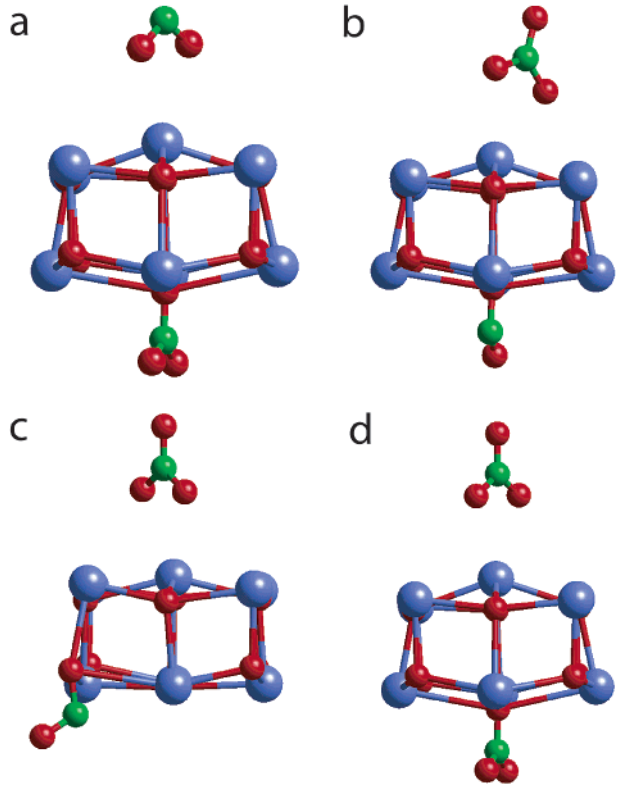


**Figure 7.** Pairwise $NO_2$ adsorption on the $(BaO)_9$ cluster in the slab configuration. (a) $(Ba-NO_2)-(O_{5S}-NO_2)$, (b) $(Ba-NO_3)-(O_{5S}-NO)$, (c) $(Ba-NO_3)-(O_{3S}-NO)$, and (d) $(Ba-NO_3)-(O_{5S}-NO_2)$. Same color code as in Figure 4.

the asymmetric and the symmetric vibrational modes, is in agreement with those found for the $NO_3^{2-}$ on MgO and CaO. The separation is here 174 $cm^{-1}$, while the corresponding separation on MgO and CaO have been reported to be 164 and 156 $cm^{-1}$, respectively.[18] However, on BaO, the peaks associated with the $NO_3^{2-}$ are shifted upward by 120 $cm^{-1}$, in comparison with the LCAO DFT results.[18] For MgO and CaO, the existence of $NO_3^{2-}$ on the surface has been experimentally verified by EPR measurements.[44,45] The wavenumber difference in the 5S configuration is found to be small and negative (asym−sym). This is expected from calculations on isolated $NO_2^-$, where we predict the asymmetric−symmetric splitting to −35 $cm^{-1}$.

*2. Adsorption of Two $NO_2$ Molecules.* The mechanism for pairwise adsorption was explored in reference 16 and shown to be surface mediated. The adsorption of one $NO_2$ creates an electron hole in the surface which promotes the adsorption of a second $NO_2$. Thus, the $NO_2-NO_2$ distance is not important for the enhancement mechanism, although it determines the lateral repulsive interaction between charged adsorbates. In this study, several configurations where the two molecules are adsorbed on opposite slab cluster facets are reported, cf. Figure 7. Figure 7a shows a nitrite−nitrate pair, where the nitrite refers to a $NO_2$ over a barium site and the nitrate is formed by $NO_2$ adsorption over a surface oxygen ion. In reference 16 a reaction scenario was proposed using three $NO_2$ molecules for the formation of the experimentally observed surface $Ba(NO_3)_2$ species and NO(g). A possible redox reaction among adsorbed $NO_2$ was suggested. The nitrite over the barium site was oxidized by the nitrate ($O_{surf}-NO_2$), forming a $NO_3-BaO-NO$ surface complex. Figure 7, parts b and c, represents configurations modeling this redox-reaction product, i.e., the ($Ba-NO_3$) and ($O_{clus}$-N−O) pair. Models 7b and 7c differ in NO adsorption site. In (b), NO is adsorbed on a five-coordinated oxygen, whereas in (c) the adsorption site is a three-coordinated edge site. To complete the picture, we also considered the nitrate−nitrate pair adsorbed on the cluster (Figure 7d).

**TABLE 5: Results of Pairwise $NO_2$ Adsorption on $(BaO)_9$ Cluster Models. (The adsorption energy is calculated toward the reference of two isolated $NO_2$ molecules. The different adsorption configurations are depicted in Figure 7.)**

| system | $E_{ads}$ [eV/2$NO_2$] |
|---|---|
| $(Ba-NO_2)-(O_{5S}-NO_2)$ | 4.21 |
| $(Ba-NO_3)-(O_{5S}-NO)$ | 4.28 |
| $(Ba-NO_3)-(O_{3S}-NO)$ | 4.38 |
| $(Ba-NO_3)-(O_{5S}-NO_2)$ | 4.17[a] |

[a] For the calculation of the adsorption energy, a NO(g) molecule is assumed to be produced from the reaction: $3NO_2 + BaO \rightarrow Ba(NO_3)_2 + NO(g)$.

The calculated adsorption energies are given in Table 5. As we demonstrated for $NO_2$ adsorption on BaO(100), there is an additional gain in adsorption energy when adding a second $NO_2$ to the system.[16] In reference 16 (for a BaO slab), the gain was calculated to 0.3 eV/2$NO_2$. In this study (for the $(BaO)_9$ cluster), the gain for the second adsorbed $NO_2$ molecule was calculated to be ∼1.4 eV/2$NO_2$. Hence, the effect of pairwise adsorption is more pronounced for the cluster models than for the periodic slab models. This is expected since the unit cell in reference 16 was small, leading to nonnegligible repulsive adsorbate interactions. Moreover, only limited surface relaxations were allowed in reference 16. The effect of pairwise adsorption has later been reported on other alkaline earth oxides, i.e., $NO_2$ on MgO(100) by Schneider et al.[17] using periodic slab models, and Bawa et al.[18] for $NO_2$ adsorption on clusters of MgO and CaO. Also, for MgO it appears that the additional energy gain is larger when modeling MgO with a cluster than with a periodic slab, 2.2 vs 1.3 eV/2$NO_2$.[17,18] Moreover, the energy gain is larger for the $2NO_2-MgO$ than for $2NO_2-BaO$. This is understandable since a single $NO_2$ molecule is only weakly physisorbed on MgO, while a chemical bond is formed when $NO_2$ adsorbs on BaO.

In reference 16 it was found that the redox-reaction product was more stable (∼0.2 eV) than both the final surface di-nitrate species and the intermediate nitrite−nitrate pair. This is also found in the present study for the structures representing (100) surface adsorption (highly coordinated surface sites, cf. Figure 7a,b,d). Furthermore, our result for NO adsorbed on a low coordinated oxygen site (Figure 7c) shows that edge effects could further enhance the adsorption energy, cf. Table 5.

In addition to the discussed configurations for the redox-reaction pair, we also explored the possibility of NO adsorbing on a barium site. However, the adsorption energy for such a configuration was significantly lower than for the conformations with NO adsorbed over oxygen sites.[46] It is therefore important to note that the stabilization calculated for simultaneous adsorption of two $NO_2$ molecules is obtained only when the odd−even chemistry of the cluster is solved. This is the case when one of the $NO_2$ molecules is adsorbed over a surface barium site and the other is adsorbed over an adjacent surface oxygen site.

A vibrational analysis was performed for the configurations in Figure 7a−c. The vibrational modes associated with the adsorbates are reported in Table 6.

*3. Summary of the Computational Vibrational Analysis.* The calculated vibrational properties are summarized in Figure 8. For the nitrates, similar vibrational modes were calculated for all investigated configurations. This was not the case for the

**TABLE 6: Calculated Wavenumbers for the Geometrical Configurations Shown in Figure 7a−c**

| configuration | $\omega_1$ sym [cm$^{-1}$] | $\omega_2$ bend [cm$^{-1}$] | $\omega_3$ asym [cm$^{-1}$] |
|---|---|---|---|
| nitrite−nitrate pair | | | |
| (Ba−$NO_2$) | 1290 | 755 | 1228 |
| ($O_{5S}$-$NO_2$) | 999 | 789, 693, 670 | 1448, 1291 |
| nitrate−nitrite pair | | | |
| (Ba−$NO_3$) | 1013 | 785, 699, 665 | 1460, 1278 |
| ($O_{5S}$-NO) | | 758 | 1397, 1140[a] |
| (Ba−$NO_3$) | 1013 | 789, 679, 675 | 1457, 1271 |
| ($O_{3S}$-NO) | | 750 | 1460, 1095[a] |

[a] For the ($O_{clus}$−NO) species, no symmetric vibration were observed. The lower value corresponds to $O_{clus}$−N stretch, while the higher value corresponds to N−O stretch.

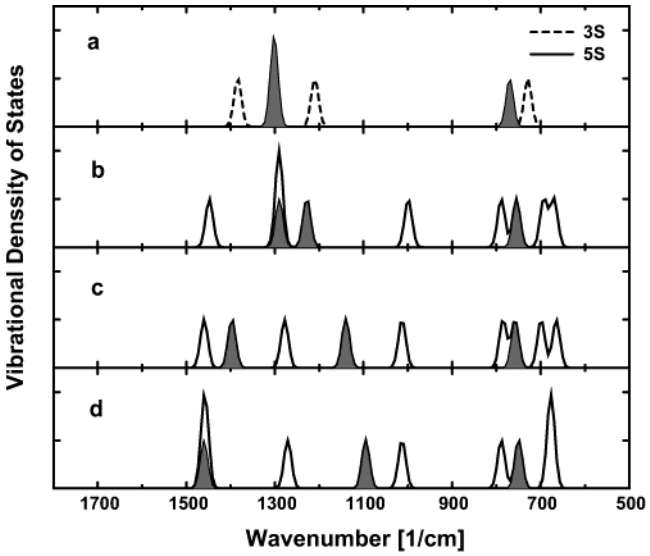


**Figure 8.** Graphical representation of the calculated vibrational frequencies in Tables 4 and 6. (a) Single $NO_2$ adsorption in the 3S and 5S configuration, (b) (Ba−$NO_2$)−($O_{5S}$-$NO_2$), (c) (Ba−$NO_3$)−($O_{5S}$-NO), and (d) (Ba−$NO_3$)−($O_{3S}$-NO). Shaded area is the vibrational contributions of the formed $NO_2^{\delta-}$ in different adsorption configurations.

**TABLE 7: Vibrational Splitting for the Different Stable Configurations of Adsorbed $NO_2$ Species Calculated from Tables 4 and 6**

| configuration | splitting [cm$^{-1}$] |
|---|---|
| 3S | 174 |
| 5S | −5 |
| (Ba−$NO_2$) | −62 |
| ($O_{5S}$-NO) | −257[a] |
| ($O_{3S}$-NO) | −365[a] |

[a] This value corresponds to the splitting between the $O_{clus}$−N and the N−O mode.

different configurations of nitrite-like species ($NO_2^{\delta-}$). Instead, the asymmetric−symmetric band splitting for the adsorbed $NO_2^{\delta-}$ species is found to be strongly dependent on adsorption configuration, cf. Figure 8 and Table 7. Comparing the 3S and 5S configurations with the (Ba−$NO_2$) configuration from the nitrite−nitrate pair adsorption, it is observed that the 3S configuration displays a positive splitting while the other two configurations display a negative splitting. Concerning the nitrite-like species formed with a cluster oxygen ion, ($O_{5S}$-NO) and ($O_{3S}$-NO), no symmetric vibrational mode is present. This is due to the asymmetric geometry which decouples the two N−O bonds, creating one N═O (double-bonded) and one N−$O_{clus}$ (single-bonded). In this case the splitting is defined as $\omega$(N−O)−$\omega$(N═O). We observe that the band splitting increases in absolute value as the integrity of a NO molecule becomes clearer. This is expected, since a partly charged NO molecule has a vibrational N−O stretch mode in the 1800−1700 cm$^{-1}$ range. Consequently, the conclusion from this analysis is that upon interconversion of oxygen atoms among the adsorbed surface species, large shifts in the vibrational spectra are expected. This splitting results from both nitrate formation and the formation of the resulting ($O_{clus}$−NO) species.

**C. Interpretation of Experimental Data.** Several vibrational spectroscopy studies of $NO_2$ storage on BaO have previously been reported.[5−7,10,11,13,14] These studies agrees that surface nitrite formation precedes the formation of surface nitrates. However, the detailed assignments may differ comparing the previous studies. Hess and Lunsford[13,14] used Raman spectroscopy to study $NO_2$ adsorption on MgO-supported BaO. Bands at 1327 and 1225 cm$^{-1}$ were assigned to the formation of N-coordinated nitrite over barium sites on the surface. Furthermore, a blue-shift of the 1327 cm$^{-1}$ band to 1337 cm$^{-1}$ was observed upon further $NO_2$ loading. The blue-shift was assigned to the formation of $NO_2^-$ ions, by comparing with a spectrum of pure $Ba(NO_2)_2 \cdot H_2O$. In contrast, Sedlmair et al.[5] have assigned bands at ∼1300 and ∼1230 cm$^{-1}$ to asymmetric and symmetric stretching modes for bridged bidentate nitrites adsorbed over barium sites, using in situ IR spectroscopy. The N-coordinated nitrites were in reference 5 assigned to peaks at 1439 and 1340 cm$^{-1}$. The interpretations of Sedlmair et al. are in agreement with studies by Fridell et al.[6,7] Furthermore, Prinetto et al.,[10] assigned asymmetric and symmetric N−O stretch modes to bands at 1220−1180 and 1330−1320 cm$^{-1}$ for ionic bidentate nitrites formed during NO/$O_2$ exposure to a Ba/$Al_2O_3$ catalyst.

Following the literature, we can assign the major peaks observed initially for BaO exposed to $NO_2$ at 30 °C, i.e., the 1319 peak and the broad band at 1250 cm$^{-1}$, to a nitro species as Hess and Lunsford,[13,14] or to a bridged bidentate or bidentate nitrite species in agreement with other reports.[5−7,10] Just as in references 13 and 14, we observe a blue-shift upon further $NO_2$ storage, i.e., the 1319 cm$^{-1}$ peak is shifting toward 1340 cm$^{-1}$. The latter interpretation of the ∼1340 cm$^{-1}$ peak together with the broad 1250 cm$^{-1}$ peak (i.e., nitrites produced upon $NO_2$ adsorption) is furthermore in agreement with our computational results for $NO_2$ adsorption, predicting a negative band splitting between the asymmetric and the symmetric N−O stretching modes, cf. Table 7. The bidentate nitrite in the $NO_2$−BaO−$NO_2$ pair configuration, cf. Figure 7a, displays similar splitting between the asymmetric and symmetric N−O stretch modes as the splitting reported from previous,[5−7,10] as well as, present experiments. However, we believe that the origin of the peak at ∼1340 is not solely from bidentate nitrites. The results for the 5S configuration, cf. Figure 5, indicates that ionic nitrites can be formed with negligible splitting in the asymmetric−symmetric modes. In the calculations for the 5S configuration, the nitrite is adsorbed with the nitrogen over an oxygen site and not over a barium site. However, the similar stability of the different $NO_2$ adsorption geometries leads to an ensemble of configurations, including N-coordinated toward both surface oxygen and barium sites.[16] Irrespectively of coordination, these species are expected to produce the vibrational signature of an ionically bonded nitrite. Thus the peak at 1340 cm$^{-1}$ may well originate from several types of adsorbed nitrites.

In the literature, assignments to monodentate nitrites are made for bands at 1500−1400 and 1200−970 cm$^{-1}$,[10] 1436 and 1347 cm$^{-1}$,[6,7] and at 1439 and 1340 cm$^{-1}$.[5] In the calculations, we only observe a significant splitting of the vibrational modes for

nitrites obtained through the redox reaction. This implies that the nitrite is incorporated into the surface, cf. Figure 7b and 7c, and the splitting results from the asymmetric geometry, observed mainly in the N−O bond lengths for the formed complex. Finally, the interpretation of nitrite formation in the low-temperature experiments is also supported by the fact that the ∼1340 $cm^{-1}$ peak is the only one observed for the $BaCO_3$ sample exposed to $NO_2$ at low temperatures, where the nitrate formation should be suppressed.

Upon heating of the stored $NO_2$ in Ar, large shifts are observed in the spectra, and additional peaks appear at 1240, 1410, 1500, and 1750 $cm^{-1}$, growing rapidly at temperatures above 250 °C (cf. Figure 1). A peak at ∼1420 $cm^{-1}$ has previously been assigned to a linear nitrite adsorbed over barium sites.[5,11] In other reports, a peak at 1475 $cm^{-1}$ has been assigned to the same species.[6,7] Conceptually, it is hard to imagine the formation of a linear nitrite. A linear $NO_2$ should involve charge donation from the $NO_2$ molecule to the surface, forming $NO_2^+$, which is a linear molecule isoelectronic with $CO_2$. Furthermore, the vibrational modes of $NO_2^+$ are expected to be blue-shifted relative to $NO_2$, which means that the peaks at ∼1420 or 1475 $cm^{-1}$ could origin from symmetric N−O stretch of $NO_2^+$. However, due to the high electronegativity of the $NO_2$ molecule, an adsorbate-to-surface charge donation is not likely to occur upon $NO_2$ adsorption on BaO.

Regarding nitrate formation, peaks at ∼1425 and ∼1332 $cm^{-1}$ have been assigned to the asymmetric and symmetric vibrational modes of monodentate nitrates over barium sites.[5] However, Fridell et al.[6,7] have assigned bands at 1560 and 1295 $cm^{-1}$ to monodentate nitrates. For the same species, Prinetto et al.[10] assign bands at 1500−1400 and 1200−970 $cm^{-1}$. Prinetto et al. also report the wavenumbers for bidentate nitrates formed upon $NO_2$ exposure to a $Ba/Al_2O_3$ catalyst to display bands at 1650−1550 $cm^{-1}$ for the $\omega$(N═O) stretch, 1320−1200 $cm^{-1}$ for the asymmetric N−O stretch, and 1050−970 $cm^{-1}$ for the symmetric N−O stretch. For the bidentate nitrate, Fridell et al.[6,7] report bands at 1594 and 1250 $cm^{-1}$. From the present calculations, wavenumbers at 1460, 1278, and 1013 $cm^{-1}$ were obtained for the nitrate species. The three investigated nitrate configurations, two bidentate and one which includes a cluster oxygen (monodentate nitrate), display similar vibrational spectra.

The presence of the 1750 $cm^{-1}$ peak is interesting since it appears in the spectra simultaneously with NO desorption, detected by mass spectrometry. A peak at 1750 $cm^{-1}$ in conjunction with a peak at ∼1260 $cm^{-1}$ is commonly associated with the formation of $N_2O_4$.[47] However, $N_2O_4$ is usually seen together with $NO_2$(g), which is not present in the current experiments, and furthermore, known to decompose at the temperatures where these peaks appear in the experiments. The 1750 $cm^{-1}$ peak is better assigned to a nitrosyl, or more precisely, a bent $Me-NO^+$ complex.[41] However, the formation of a metal coordinated nitrosyl species implies charge donation from the NO molecule to the surface metal cation in conjunction with charge back-donation to the NO $\pi^*$ orbital. This type of bond is not likely to form in case of NO adsorption over a $Ba^{2+}$, because of the lack in back-donation capability. A weak $NO-Ba^{2+}$ bond is, moreover, predicted in the present calculations.[46] Instead the 1750 $cm^{-1}$ peak could be due to NO adsorbed on an $O^-$ site, forming a $(O^{2-}-NO^+)$ surface complex. This site would allow for back-donation into the $NO^+$ $\pi^*$ orbital. The binding can be seen to result from pairing the unpaired NO $\pi^*$ electron with an unpaired surface $O^-$ electron, creating a covalent chemical bond. Snis and Panas[48] calculated the N−O stretch mode for NO adsorbed on $O^-$ edge sites on CaO to be at 1765 $cm^{-1}$, using an embedded cluster model and an ab initio multi-configurational wave function method. Our calculations (cf. Table 6) of the ($O_{3S}$-NO) species show lower frequencies (1460 and 1095 $cm^{-1}$). Several reasons could exist for this difference. The cluster model employed allows for large structural relaxations in the BaO cluster upon the formation of the ($O_{clus}-NO$) species.

From experiments it is clear that the splitting observed in the spectra is a sign of nitrate formation, triggered by the temperature increase. This scenario is supported by our calculations, where an increased vibrational splitting was calculated for the interconversion of oxygen atoms among the adsorbates, resulting in coexistence of nitrates and nitrites on the surface, illustrated in Figure 8. In Figure 8 it is shown that both nitrite formed upon redox reaction and the adsorbed nitrate display vibrational modes at similar wavenumbers. The similarity in vibrational properties for several different adsorption configurations (especially for nitrites), make experimental assignments of specific surface species ambiguous.

In the spectra recorded for BaO exposed to $NO_2$ at 250 °C, peaks were monitored at 1500, 1420, 1380, and 1260 $cm^{-1}$ (Figure 2), indicating rapid surface reactions forming nitrate−nitrite pairs. In this case we also have to consider the presence of $NO_2$ during the whole experiment, leading to a higher probability of nitrate formation, both on the surface and in the bulk. As we are mainly interested in the initial $NO_2$ storage mechanism, the spectra taken at this temperature are included to illustrate the onset of surface reactions at intermediate temperatures. Therefore, no attempt to assign the peaks in these spectra have been made. However, some conclusions can be made. On the time scale of the experiments, no 1330 $cm^{-1}$ peak, indicating single adsorbed nitrites is observed. Formation of bulk nitrates is believed to occur at this temperature, seen as a large peak at ∼1380.[49] Similar reasoning holds for the spectra taken for $NO_2$ exposure to $BaCO_3$ (Figure 3), which is mainly used as reference to the low-temperature experiments made for BaO. This means that limited attempts are made here to assign peaks in these spectra. However, it is interesting that at low temperature, similar peaks are found for the BaO powder sample as for $BaCO_3$, indicating nitrite formation over barium sites.

## Conclusions

DRIFT experiments in conjunction with vibrational analysis using DFT calculations have been employed to study different configurations of charged $NO_x$ ($x = 1,2,3$) species formed upon adsorption of $NO_2$ on BaO.

For BaO exposed to $NO_2$ at low temperatures, only peaks associated with nitrites are observed in the spectra. This conjecture is supported from the computational analysis of single $NO_2$ adsorbed on the cluster, showing a negligible asymmetric−symmetric wavenumber splitting. In the vibrational analysis, it was found that the characteristic vibrations of a $NO_3^{2-}$ species previously reported for $NO_2$ adsorption on $(MgO)_9$ and $(CaO)_9$[18] also are present for $NO_2$ adsorption on a 3-fold coordinated oxygen site on $(BaO)_9$. The experiments, however, did not reveal this species. This is probably due to the fact that nitrite formation is energetically favored on this compound leading to higher intensity for the nitrite species. Furthermore, the formation of nitrites should produce $O^-$ sites on the surface, which should be possible to verify experimentally using EPR measurements.

Upon pairwise adsorption of $NO_2$ on the $(BaO)_9$ cluster, a significant additional energy gain is calculated for the second $NO_2$ molecule (1.4 eV). This indicates that an important step for the overall storage capacity is the initial nitrite formation.

An enhanced nitrite stability increases the probability of pair formation, which is the most stable form of $NO_x$ species on the surface and enhances the loading capability significantly. Previous calculations[16] predict a redox reaction among adsorbates forming nitrate−nitrite pairs on the surface. In the present experiments, the proposed redox reaction is believed to occur when the stored $NO_2$ is heated in Ar. During the heating ramp, an interconversion of oxygen atoms among adsorbates forming nitrates coexisting with nitrites on the surface is observed in the spectra. This is supported by the theoretical vibrational study, which predicts large shifts upon oxygen transfer among adsorbates (Figure 8).

Finally, the sensitivity in the vibrational band splitting of the nitrite-like species ($NO_2^{\delta-}$) with respect to different adsorption configurations have been analyzed by calculations of single and pairwise adsorption of $NO_2$ on $(BaO)_9$. The analysis demonstrates the difficulty in assigning stored $NO_x$ species by vibrational spectroscopy.

**Acknowledgment.** Financial support from the Swedish Research Council (P.B. and I.P.) is gratefully acknowledged, as are constructive discussions with Prof. Bengt Andersson and Prof. Bengt Kasemo. The calculations have been performed on IBM SP at PDC, Stockholm, Sweden. Prof. Sten Eriksson and Marcus Valkeapää are acknowledged for providing us with a glovebox for transferring the BaO sample into the reaction chamber. This work has been performed within the Competence Centre for Catalysis, which is financially supported by the Swedish Energy Agency, Chalmers and the member companies: AB Volvo, Johnson Matthey CSD, Saab Automobile Powertrain AB, Perstorp AB, MTC AB, Eka Chemicals, and the Swedish Space Corporation.

## References and Notes

(1) Takahashi, N.; Shinjoh, H.; Iijima, T.; Suzuki, T.; Yamazaki, K.; Yokota, K.; Suzuki, N.; Miyoshi, N.; Matsumoto, S.; Tanizawa, T.; Tanaka, T.; Kasahara, K. *Catal. Today* **1996**, *27*, 63.

(2) Bögner, W.; Krämer, M.; Krutzcsh, B.; Pischinger, S.; Voigtländer, D.; Wenninger, G.; Wirbeleit, F.; Brogan, M.; Brisley, R.; Webster, D. E. *Appl. Catal. B* **1995**, *7*, 153.

(3) Fridell, E.; Skoglundh, M.; Johansson, S.; Westerberg, B.; Thörncrona, A.; Smedler, G. *Stud. Surf. Sci. Catal.* **1998**, *116*, 537.

(4) Fridell, E.; Skoglundh, M.; Westerberg, B.; Johansson, S.; Smedler, G. *J. Catal.* **1999**, *183*, 196.

(5) Sedlmair, C.; Seshan, K.; Jentys, A.; Lercher, J. A. *J. Catal.* **2003**, *214*, 308.

(6) Fridell, E.; Persson, H.; Westerberg, B.; Olsson, L.; Skoglundh, M. *Catal. Lett.* **2000**, *66 (*1−*2)*, 71.

(7) Fridell, E.; Persson, H.; Olsson, L.; Westerberg, B.; Amberntsson, A.; Skoglundh, M. *Top. Catal.* **2001**, *16/17*, 133.

(8) Olsson, L.; Persson, H.; Fridell, E.; Skoglundh, M.; Andersson, B. *J. Phys. Chem. B* **2001**, *105*, 6895.

(9) Lietti, L.; Forzatti, P.; Nova, I.; Tronconi, E. *J. Catal.* **2001**, *204*, 175.

(10) Prinetto, F.; Ghiotti, G.; Nova, I.; Lietti, L.; Tronconi, E.; Forzatti, P. *J. Phys. Chem. B* **2001**, *105*, 12732.

(11) Westerberg, B.; Fridell, E. *J. Mol. Catal. A: Chem.* **2001**, *165*, 249.

(12) Roidrigues, F.; Juste, L.; Potvin, C.; Tempé, J.; Blanchard, G.; Djéga-Mariadassou, G. *Catal. Lett.* **2001**, *72* (1−2), 59.

(13) Hess, C.; Lunsford, J. H. *J. Phys. Chem. B* **2002**, *106* (25), 6358.

(14) Hess, C.; Lunsford, J. H. *J. Phys. Chem. B* **2003**, *107* (9), 1982.

(15) Prinetto, F.; Ghiotti, G.; Nova, I.; Lietti, L.; Tronconi, E.; Forzatti, P. *J. Phys. Chem. Chem. Phys.* **2003**, *5*, 4428.

(16) Broqvist, P.; Panas, I.; Fridell, E.; Persson, H. *J. Phys. Chem. B* **2002**, *106*, 137.

(17) Schneider, W. F.; Hass, K. C.; Miletic, M.; Gland, J. L. *J. Phys. Chem. B* **2002**, *106* (30), 7405.

(18) Bawa, F.; Broqvist, P.; Panas, I. In preparation.

(19) Broqvist, P.; Grönbeck, H.; Panas, I. *Surf. Sci.*, in press.

(20) Grönbeck, H.; Broqvist, P. *J. Chem. Phys.* **2003**, *119* (7), 3896.

(21) Schneider, W. F.; Li, J.; Hass, K. C. *J. Phys. Chem. B* **2001**, *105*, 6972.

(22) Hinz, A.; Skoglundh, M.; Fridell, E.; Andersson, A. *J. Catal.* **2001**, *201*, 247.

(23) Car, R.; Parrinello, M. *Phys. Rev. Lett.* **1985**, *55*, 2471.

(24) Andreoni, W.; Curioni, A. *Parallel Computing* **2000**, *26*, 819.

(25) Marx, D.; Hutter, J. *Modern Methods and Algorithms in Quantum Chemistry;* Forschungzentrum Juelich NIC Series, Vol. 1, 2000.

(26) CPMD v3.5 Copyright IBM Corp 1990−2001, Copyright MPI fuer Festkoerperforschung Stuttgart 1997−2001.

(27) Perdew, J. P.; Zunger, A. *Phys. Rev. B* **1981**, *23*, 5048.

(28) Ceperly, D. M.; Adler, B. J. *Phys. Rev. Lett.* **1980**, *45*, 566.

(29) Perdew, J.; Burke, K.; Ernzerhof, M. *Phys. Rev. Lett.* **1996**, *77*, 3865.

(30) Troullier, N.; Martins, J. L. *Phys. Rev. B* **1992**, *46*, 1754.

(31) The cutoff radii (in atomic units) are the following: Ba s(1.5) local, p(1.5) and d(2.5); O s(1.3) local and p(1.3); and N s(1.2) local and p(1.2).

(32) Barnett, R.; Landman, U. *Phys. Rev. B* **1993**, *48*, 2081.

(33) Pulay, P. *Chem. Phys. Lett.* **1980**, *73*, 393.

(34) Hutter, J.; Luthi, H. P.; Parrinello, M. *J. Comput. Mater. Sci.* **1994**, *2*, 224.

(35) All calculations were performed sampling only the gamma-point. For the bulk calculations of BaO, a 64 atom unit cell was used.

(36) Delley, B. *J.Chem. Phys.* **1990**, *92*, 508.

(37) Delley, B. *J. Chem. Phys.* **2000**, *113*, 7756.

(38) Greenwood, N. N.; Earnshaw, A. *Chemistry of the Elements;* Pergammon Press: Oxford, U.K., 1984.

(39) Nordling, C.; Österman, J. *Physics Handbook*; Studentlitteratur, Lund, Sweden, 1987.

(40) Königstein, M.; Catlow, C. R. A. *J. Solid State Chem.* **1998**, *140*, 103.

(41) Hadjiivanov, K. I. *Catal. Rev.—Sci. Eng.* **2000**, *42* (1&2), 71.

(42) Bawa, F.; Panas, I. *Phys. Chem. Chem. Phys.* **2002**, *4*, 103.

(43) Karlsen, E. J.; Nygren, M. A.; Petterson, L. G. M. *J. Phys. Chem. B* **2003**, *107*, 7795.

(44) Paganini, M. C.; Martino, M. C. P.; Giamello, E. *J. Phys. Chem. B* **2002**, *106* (48), 12531.

(45) Valentin, C. D.; Pacchioni, G.; Chiesa, M.; Giamello, E.; Abbet, S.; Heiz, U. *J. Phys. Chem. B* **2002**, *106*, 1637.

(46) The energy for the Ba−NO configuration was about 2 eV over the stable $[O-NO]^-$ configuration. Short molecular dynamics simulations were performed to find additional bridge sites for the NO molecule. All these configurations came out significantly higher in energy than the stable ones reported in Table 5.

(47) Domenech, J. L.; Andrews, A. M.; Belov, S. P.; Fraser, G. T.; Lafferty, W. J. *J. Chem. Phys.* **1994**, *100* (10), 6993.

(48) Snis, A.; Panas, I. *Surf. Sci.* **1998**, *412/413*, 477.

(49) Coronado, J. M.; Andersson, J. A. *J. Mol. Catal. A: Chem.* **1999**, *138*, 83.